

CHAPTER 11

Colloids and Molecular Organization in Liquids

11.1 Introduction

In many biological systems and some polar polymers, the organization which is observed in the solid is a consequence of processes of pre-assembly occurring in the solution or melt phase prior to solid formation. In Chapter 10 the effects of surfaces on the free energy were considered and in Chapter 3 the possibility of pre-assembly through liquid crystalline phase formation was discussed. An important class of liquid crystalline materials that was not considered in detail in Chapter 3 are *lyotropic* molecules. Molecules such as stearic acid ($\text{CH}_3(\text{CH}_2)_{16}\text{CO}_2\text{OH}$) and palmitic acid ($\text{CH}_3(\text{CH}_2)_{14}\text{COOH}$) are examples of this type of molecule.¹ The molecular structure is made up of a polar end that is hydrophilic and a non-polar hydrophobic group that usually contains a hydrocarbon chain. The polar group will be soluble in water, whereas the hydrocarbon tail will be insoluble. Attempting to disperse these molecules in water, we find that they exhibit a limited solubility before phase separating. The free energy of the system is favoured by the stearic acid separating out at the water–air interface (Figure 11.1), this being the usual action of a soap.

The segregation of the molecules to the interface is a consequence of the necessity to balance the free energy of the interface. The problem can be considered in terms of a Gibbs surface, which is an arbitrary plane defined in terms of a plane between the two partly miscible liquids. The Gibbs surface is

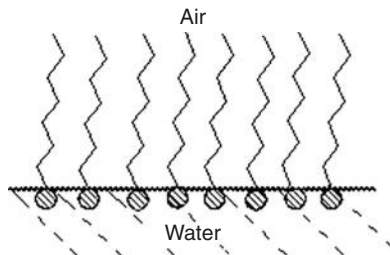


Figure 11.1 Schematic of the organization of stearic acid at the air–water interface.

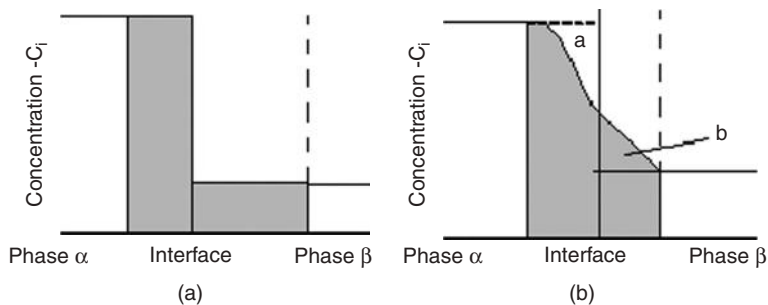


Figure 11.2 Schematic of the surface excess distribution of a surface active species across an interface between two immiscible liquids. (a) Ideal distribution showing ideal shape interface. (b) Distribution across interface. The Gibbs interface is an arbitrary line which in the first case represents the solubility in the two phases α and β and the second (b) is constrained so that the areas are equal.¹

the interfacial region between the two phases α , β and has a finite thickness implying that there is some solubility of one liquid in the other (Figure 11.2). This is the case for a molecule such as stearic acid that at very low concentrations will be soluble in water but is also soluble in oil.

11.2 Ideal Non-mixing Liquids

The theory considers the distribution of surface active species across an interface between two essentially immiscible liquids (Figure 11.2). The ideal situation is depicted in Figure 11.2a; however, in practice there will be the possibility of a distribution of the surface active molecules across the interface, reflecting that the interface has a finite thickness. The distribution of the surface active component is shown by the shaded area, and in Figure 11.2a there is a clear change in concentration at the Gibbs surface, whereas in the other situations there is distribution of concentration. The generalized theory considers the effect of the surface excess Γ_i on the surface tension γ . The adsorption of a component at the interface will be defined by a decrease in the surface tension γ . We can define the so-called spreading pressure π as

$$(\gamma_0 - \gamma) = \pi \quad (11.1)$$

where γ_0 is the surface tension of the interface in the absence of the surface active component. Using Helmholtz energy instead of Gibbs free energy:

$$\partial A^\sigma = -S^\sigma \partial T - P \partial V^\sigma + \gamma \partial a + \sum_i \mu_i \partial n_i \quad (11.2)$$

where the parameters with superscript σ are the values appropriate for the surface.

Integration of eqn (11.2), keeping the intensive variables constant (*i.e.* T, P, μ_i, γ), yields

$$A^\sigma = -PV^\sigma + \gamma_a \partial a + \sum \mu_i \partial n_i \quad (11.3)$$

Equation (11.3) can be differentiated to obtain the total derivative:

$$\partial A^\sigma = -P\partial V^\sigma - V^\sigma \partial P + \gamma \partial a + a \partial \gamma + \sum \mu_i \partial n_i + \sum n_i \partial \mu_i \quad (11.4)$$

Subtraction of eqn (11.4) from (11.2) gives

$$S^\sigma \partial T - V^\sigma \partial P + a \partial \gamma + \sum_i n_i^\sigma \partial \mu_i = 0 \quad (11.5)$$

If the conditions are isothermal then with T constant and $V^\sigma \approx 0$, we obtain

$$a \partial \gamma + \sum_i n_i^\sigma \partial \mu_i = 0 \quad (11.6)$$

which rearranges to

$$-a \partial \gamma = \sum_i n_i^\sigma \partial \mu_i \quad \text{and} \quad -\partial \gamma = \sum_i \frac{n_i^\sigma \partial \mu_i}{a} \quad (11.7)$$

which can be rearranged to have the form

$$-\frac{\partial \gamma}{\partial \mu_i} = \sum_i \frac{n_i^\sigma}{a} \quad (11.8)$$

which is the number of moles per unit area at the surface and leads to the so-called Gibbs equation:

$$-\frac{\partial \gamma}{\partial \mu_i} = \sum_i \Gamma_i \quad (11.9)$$

which is the surface excess Γ_i in mol m^{-2} . For a two-component system, *i.e.* a solvent and solute, which is the situation for a soap dispersed in water with an air interface, then

$$-\partial \gamma = \Gamma_1 \partial \mu_1 + \Gamma_2 \partial \mu_2 \quad (11.10)$$

In this situation it is reasonable to assume that the water cannot cross the interface into the air, but the soap molecule can be located both in the water and air regions. In this case we let Γ_1 , the excess area due to component 1, be zero:

$$-\partial \gamma = \Gamma_2 \partial \mu_2 \quad (11.11)$$

and $\mu_2 = \mu_2^0 + RT \ln(a_2)$, in which a is the activity of the distributed component and μ_2^0 is a constant. Differentiating eqn (11.11) yields

$$\partial\mu_2 = RT\partial\ln(a_2) \quad (11.12)$$

which is referred to as the Gibbs absorption isotherm:

$$-\partial\gamma = \Gamma_2 RT\partial\ln(c_2) \quad (11.13)$$

This equation is often rearranged using $-\partial\gamma = \Gamma\partial\mu$ and $\partial\mu = RT\partial\ln(a)$ to give the surface excess area as

$$\Gamma = -\frac{\partial\gamma}{\partial\mu} = -\frac{1}{RT} \frac{\partial\gamma}{\partial\ln(c)} \text{ or } \Gamma = \frac{-c}{RT} \frac{\partial\gamma}{\partial c} \quad (11.14)$$

The implications of these equations are as follows:

- If $\gamma \downarrow$ as $c \uparrow$, then $\partial\gamma/\partial c$ is negative so Γ is positive and the component is adsorbed at the interface.
- If $\gamma \uparrow$ as $c \uparrow$, then $\partial\gamma/\partial c$ is positive so Γ is negative and depletion of the component occurs at the interface.

This latter situation occurs in the case of some ionic solutions, where as a result of solvation of the species, it would prefer to stay in the bulk rather than at the surface. In the case of a soap, the gain in energy for the hydrophobic tail being transferred across the interface is greater than the solvation energy and segregation tends to occur. In this latter situation, $\pi = (\gamma^0 - \gamma)$ can be expressed as being proportional to the concentration c so that $\pi = kc$ and $k = \pi/c$, so that $\gamma^0 - \gamma = kc$ and $\gamma = \gamma^0 - kc$ leading to $\partial\gamma/\partial c = -k = -\pi/c$, and

$$\Gamma = -\frac{c}{RT} \left(\frac{\partial\gamma}{\partial c} \right) = \frac{-c}{RT} \left(\frac{-\pi}{c} \right) \text{ and } \Gamma = \frac{\pi}{RT} \quad (11.15)$$

The spreading pressure adsorption (mol m^{-2}) is thus $\pi/\Gamma = RT$. If we let $1/\Gamma = \sigma$ ($\text{m}^2 \text{ mol}^{-1}$), then $\pi\sigma = RT$, *i.e.* the spreading pressure \times area occupied by 1 mole = RT . This is the two-dimensional analogue of the ideal gas equation and implies that molecules can move around a surface in the same way that a gas moves around in a three-dimensional solid.

11.3 Minimum Surface Energy Conditions

Although we are primarily concerned with phases which are created within a solution or a solid, looking at an air-liquid interface can help with understanding the conditions that occur in the former conditions. Depending on the surface tension, the vapour-liquid interface will adopt a curvature that reflects the balance of forces that exist in the surface (Figure 11.3).

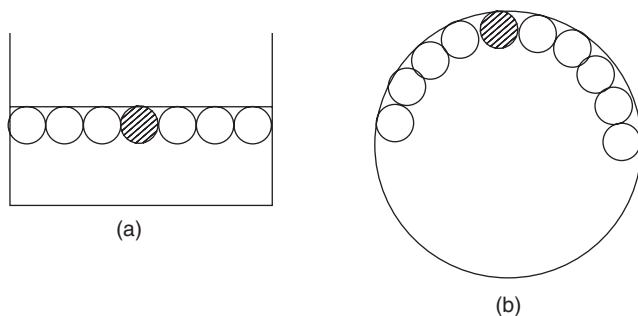


Figure 11.3 Schematic of a plane and curved surface.

In a curved surface (Figure 11.3b), the coordination of any individual molecule will be less than in a planar surface (Figure 11.3a). The coordination is less at a curved surface with the result that there is a greater tendency for the molecules to be able to leave the surface and the effective vapour pressure is higher. Thus using

$$\Delta G = VdP - SdT + \sum_i \mu_i dn_i + \gamma dA \quad (11.16)$$

we can define $\mu_i = (dG/dn_i)_{P,T,n_i,a}$ for a flat surface. Thus for a small drop, the addition of a small amount of material dn_i changes the volume and therefore the area. The addition of dn_i to a drop of radius r leads to a change in volume $dV = \sum \bar{V}_i dn_i = 4\pi r^2 dr$ where $\bar{V}_i (=dV/dn_i)$ is the partial molar volume change, and can be expressed for a sphere as

$$dA = 8\pi r dr = \frac{2(4\pi r^2 dr)}{r} = \frac{\sum_i 2\bar{V}_i dn_i}{r} \quad (11.17)$$

Substitution in eqn (11.16) gives

$$dG = VdP - SdT + \sum_i \mu_i dn_i + \frac{\left(\sum_i 2\bar{V}_i dn_i\right)}{r} \quad (11.18)$$

$$= VdP - SdT + \sum_i \left(\frac{2\bar{V}_i \gamma}{r} + \mu_i\right) dn_i \quad (11.19)$$

We can define for a simple curved surface

$$\mu'_i = \left(\frac{dG}{dn_i}\right)_{T,P,n_i} \quad (11.20)$$

so that $\mu'_i = 2\bar{V}_i \gamma / r + \mu_i$ which is equal to the difference in the curved surface and the plane surface, and $\mu'_i - \mu_i = 2\bar{V}_i \gamma / r$. One can compare the equations for

the plane and curved surfaces: $\mu_i = \mu_i^0 + RT \ln P_i^0$ for a plane surface and $\mu_i = \mu_i^0 + RT \ln P_i$ for a curved surface. Thus $\mu_i^0 + RT \ln P_i - \mu_i^0 - RT \ln P_i = 2\overline{V}_i\gamma/r$ and $RT(\ln P_i/\ln P_i^0) = 2\overline{V}_i\gamma/r$ which leads to $\ln P_i/\ln P_i^0 = 2\overline{V}_i/RT(r)$. These equations illustrate the observation that droplet and phase separated systems will naturally tend to form a curved surface to minimize the free energy.

11.4 Langmuir Trough^{1,2}

In this monograph, we are primarily interested in organization in the solid state; however, since solids are formed from either melts or often solutions it is appropriate to understand the conditions under which pre-assembly of ordered phases is possible in the liquid phase. The pioneering work of Langmuir has helped us gain an insight into the way molecules can organize at liquid–air interfaces and in particular the biologically important water–air interface. The most common method of studying the surface is using a Langmuir balance^{3,4} (Figure 11.4).

The trough is usually constructed from a ceramic and filled to the brim with the substrate (water). The substance to be investigated is carefully added to the trough. In order to define the surface area, a series of movable bars are placed across the surface of the liquid (water). There is usually one bar that is movable and controlled by a screw or pulley. This bar can be moved up and down the trough and allows the area of the surface to be varied. Reduction of the area by movement of the static and movable bars together squashes the molecules trapped in the surface and leads to an increase in the surface pressure. The pressure or force in the surface is easily measured using a piece of filter paper, suspended so as to lie vertically in the surface and its mass is measured using a delicate balance. Typical plots that are obtained are shown in Figure 11.5.

Large molecules, such as sodium stearate, which have no side chains are able to pack into a single monolayer as the pressure is increased. A complete

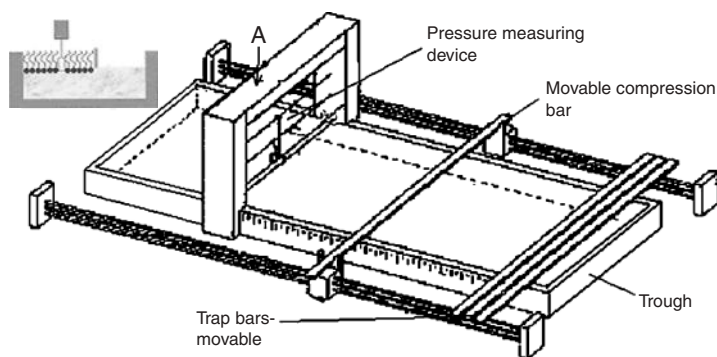


Figure 11.4 Schematic of a Langmuir trough. The marks on the side of the trough indicate distance and hence area of the surface. The inset indicates the compression of the molecules by the moving barrier.⁵

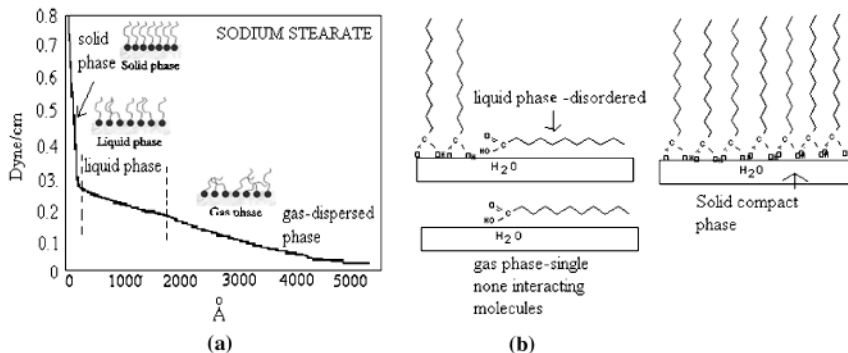


Figure 11.5 (a) Pressure area plot for sodium stearate and (b) schematic diagrams for the various states of compaction of the molecules in the surface. The division of the areas follows the nomenclature of Langmuir.¹

compressed monolayer will be created at the solid–liquid line and this is essentially a crystalline solid. Below the liquid–gas line, the molecules are more disordered in the surface and at various stages will resemble liquid-like order and, in the extreme, a gas.

11.5 Langmuir–Blodgett Films^{3,4}

Over the last twenty years, a vast amount of research has been carried out on ordered films, prepared using a Langmuir trough and a dipping method. The technique involves moving a substrate through the layer that has been compressed to be close to the ‘solid’ condition. The layers that are picked off from the surface can then be assembled to produce ‘idealized’ structures that mimic in many cases those found in nature. The process is shown schematically in Figure 11.6. The molecules are first compressed into a monolayer on the liquid surface (Figure 11.6a). A plate, usually a quartz slip, is lifted from below the surface, and moving through the monolayer (Figure 11.6b) picks up a single layer of pre-ordered molecules. If the plate is then pushed back through the surface, a further monolayer is deposited (Figure 11.6c) and so on (Figure 11.6d). Many tens of monolayers have been deposited by this method producing well-organized model structures. The structure of the layers alternates, as the first layer will have the hydrocarbon chains sticking up from the surface and the carbonyl head groups attached to the glass. This hydrophobic surface of the glass slip coated with the monolayer of molecules is then wetted as the plate is returned to the bath by the hydrocarbon chains in the surface monolayer. The molecules in the surface will align with the hydrocarbon chains of the first monolayer changing the surface to being hydrophilic by depositing the second layer in the reverse sense to the first layer. Removal of the plate will once more coat the plate with a further layer aligned in the same sense as the first layer and make the surface hydrophobic. This will then be repeated on

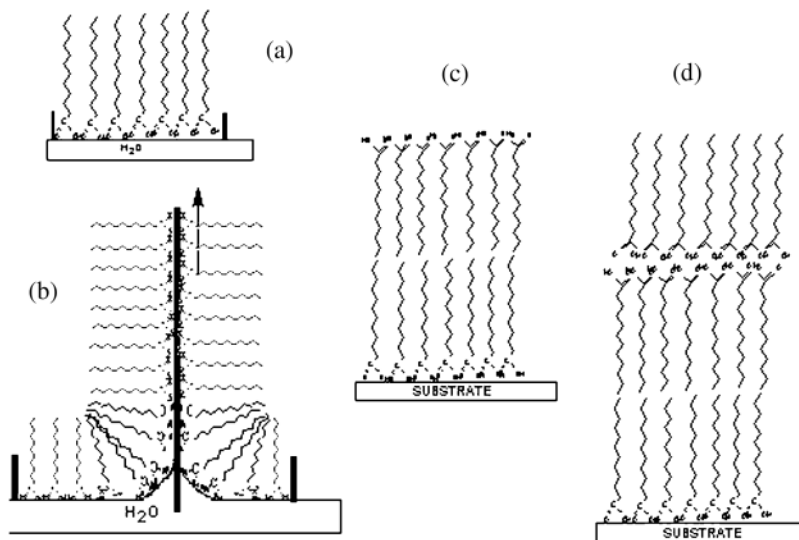


Figure 11.6 Various stages of Langmuir–Blodgett film deposition.

subsequent dipping. The substrates are usually hydrophilic (glass or quartz for optical studies, silver and gold (conductive substrates), silicon or gallium arsenide plates (semiconductive)) or hydrophobic (mica or organically modified glass).

The bilayer structure (two layers organized back to back) is similar to that found in virtually all biological cell structures and forms an effective barrier between two aqueous phases. The layers instead of adopting a planar structure will curve to minimize the energy. The result of the curvature is to form a closed surface with the hydrophilic head groups in contact with the aqueous environment both within and outside the cell. The molecules that can be deposited by this method include many amphiphilic molecules. These molecules usually contain a non-polar hydrocarbon-based chain: alkylbenzene, benzenedodecyl, lauryl, stearic, palmitic oleic, hydrogenated tallows and other fatty acids. The polar head group is usually a sulfate, phosphate, carboxylic acid or amine. Counter ions often will include sodium, potassium or ammonium ions. These molecules can distribute themselves across an interface and change the surface energy.

11.6 Micelle Formation^{1,2}

The situation that exists in the trough is rather more complex than this simple picture portrays. In very dilute solution, the molecules may be soluble in the water and hence there is a distribution between the bulk and surface. However, as the concentration is increased the possibility of the surfactant molecules

self-aggregating arises. At a critical concentration, the *critical micelle concentration* (CMC), molecular-scale particles are formed in the solution. These molecular-scale particles are called *micelles* and in the simplest form have a spherical shape, with a diameter that is approximately the extended length of the hydrophobic chain. In the case of sodium stearate, there are approximately 50 molecules contained within this spherical micelle structure. Because it has a curved interface with water it will represent a low-energy structure. Because they are of molecular dimensions they will not scatter light and solutions appear clear; however, many physical properties of the solution are changed as a consequence of their presence. The process of micelle formation is illustrated in Figure 11.7. Because the formation of micelles depends on the solubility of the surfactant in the dispersing media, there exists a critical micelle temperature (CMT) below which a micelle can exist and above which it does not exist. There is also another temperature that exists in the surfactant system known as the Krafft point. The Krafft point marks a transition between the dissolution of the soap to form ions and its dissolution to form micelles. The solubility of soap increases sharply with temperature once micelles have appeared by a process that can only be described as self-solubilization that packs more solute into micelles. The Krafft temperature and CMT are closely related.

A micelle will contain a number of molecules, the exact number depending upon the alkyl chain length. As the chain length is increased, so the number of molecules contained in the micelle will proportionally increase:

<i>Number of C atoms in detergent chain, n</i>	<i>Number of molecules in micelle, m</i>
12	33
14	46
16	60
18	78

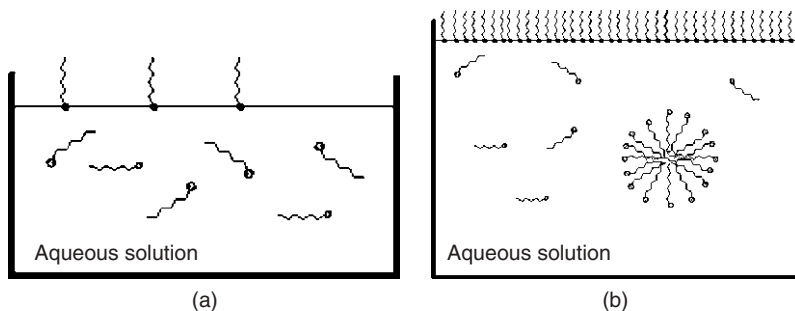


Figure 11.7 Distribution of molecules between the bulk and surface: (a) at a concentration well below the CMC; (b) at a concentration well above the CMC.

Colloidal systems can be divided into two types. *Lyophilic* colloids (solvent loving) are true solutions of a single large molecule or aggregate. They are formed when solute and solvent are brought together and are stable indefinitely. *Lyophobic* (solvent hating) do not form spontaneously and generally need some additional factor to stabilize them. If left long enough the two phases may separate. The general discussion of colloidal systems is beyond the scope of this monograph and the reader is referred to one of the texts listed at the end of this chapter for more detailed discussions on this topic. *Lyophobic* systems can demonstrate the way in which adsorbed molecules on a surface can influence the habit of growth of inorganic crystals and are important in understanding bio-mineralization.

11.7 Stability Energy and Surface Area Considerations in Colloids

The behaviour of the two types of system is reflected in the energy of interaction between the molecules and the dispersing solvent. *Lyophilic* systems are constituted from large molar mass molecules, such as casein, dissolved in a solvent, such as water, to produce a single-phase colloidal solution, milk. The polymer chain is fully solvated by the solvent molecules, all segments are in equilibrium with the surrounding media or solvation shell and the system is thermodynamically and kinetically stable. In *lyophobic* systems the surface tension force acts parallel to the surface pulling inwards to oppose the spreading of the surface. Assuming that the volume is not otherwise constrained, then the smallest surface area for a given volume is a sphere. The total surface energy of the system is equal to the product of the surface tension and the surface area. Suppose we divide a single particle into a series of smaller spheres. For a given mass of the dispersed phase there will be $n = m/4\pi r^3 \rho$ particles, where r is the average radius and ρ is the density. Therefore n is proportional $1/r^3$. The total area of these n particles is $= n \times 4\pi r^2 \propto n \times r^2 \propto r^2/r^3$. Therefore the total surface area is proportional to $1/r$. Therefore as we decrease the radius of the particle we increase the total surface area and hence the total surface energy of the system. Therefore the system becomes less thermodynamically stable in the absence of other factors. Specific surface area A_{sp} is defined as the ratio of the total surface area to the total mass: $A_{sp} = n \times 4\pi r^2 / n \times 4/3\pi r^3 \rho = 3/r\rho$. Although a system may be thermodynamically unstable, many colloids have significant long-term stability (kinetic stability) as a result of a high activation energy for change. Total surface energy for 1 mol of particles of radius 10^{-7} cm is 4 kJ mol^{-1} and should be compared with the activation energy for viscous flow or bond strength, 40–100 kJ mol^{-1} .

11.8 Stability of Charged Colloids

Many colloidal systems and in particular biological systems contain oligomers and macromolecules that can carry a charge. A typical colloidal solution

consists of the continuous phase, usually water, a colloidal electrolyte particle and a low molecular weight univalent electrolyte, *i.e.* a simple salt. We designate the colloidal particle as a macroion PX_z , where P is the particle itself carrying z positive charges and is maintained electrically neutral by z counter anions X^- . When such a colloid system is introduced into a vessel separated by a membrane, as in an osmometer, then the small ions M^+ , X^- can pass through the membrane but the macro ions (colloid itself) cannot. At equilibrium (Donnan equilibrium):

$$\begin{array}{ccc} M^+X^- & & M^+X^-P^{z+} \\ \beta \text{ phase} & & \alpha \text{ phase} \\ (a_{M,\alpha})(a_{X,\alpha}) = (a_{M,\beta})(a_{X,\beta}) & & \text{Ion activity product} \end{array}$$

In practice, M or X^- are not evenly distributed but are influenced by the presence of P^{z+} , the colloidal species and the more colloid or macroions present and the higher the charge they carry z , then the greater the unevenness of the distribution of the M^+ ion. In practice, the membrane itself generally becomes polarized because of the macroions on one side and this is similar to the natural membranes in living systems. In dialysis, the Donnan equilibrium allows the removal of ions and traces of impurities. This is a fascinating topic that we do not have space to explore in detail in this monograph.

11.9 Electrical Effects in Colloids

The kinetic effects in lyophilic systems are usually associated with the charge carried by the particle. Proteins, for example, acquire charge through ionization of carboxyl and amino groups to give $-\text{COO}^-$ and $-\text{NH}_3^+$ ions. The charge on the protein is thus pH dependent because $-\text{COOH}$ is a weak acid and $-\text{NH}_2$ is a weak base. At low pH the protein will be positively charged and at high pH will be negatively charged. There is an isoelectric point where there will be no charge on the molecule.

With lyophobic systems charge can also readily be acquired. Hydrocarbon droplets in water acquire a negative charge by preferential adsorption of anions, *e.g.* OH^- are less hydrated than the cations H^+ and have greater polarizing power. Even air bubbles can acquire charge and stick to the side of a drinking glass.

11.10 Electrical Double Layer^{1,2}

When we have a charged surface in the absence of thermal motion, the charge would be neutralized by adsorption of an equal and opposite number of charged ions (counter ions or gegen ions). In fact, thermal motion prevents formation of such a compact double layer and in practice there is a distribution of counter ions (a screening effect) and a distribution of counter ions in the vicinity of the surface, such that the electrical potential gradually falls to zero at

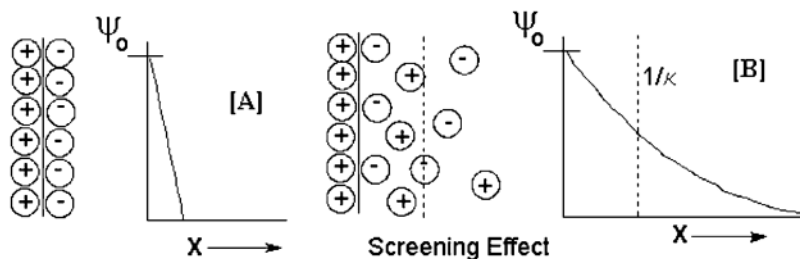


Figure 11.8 Schematic of the ion distribution close to an interface. It is assumed that the particle dispersed in the aqueous phase carries a positive charge and there will be a distribution of negative counter ions in solution. In addition, cations may be present and aid the charge balance.

long distances from the particle surface. This is known as a diffuse double layer and it is possible theoretically to treat the situation quantitatively in a number of ways (Figure 11.8). The first approach is to assume that the ions are not in motion and that they balance out at the interface. This leads to the Gouy–Chapman regime.⁵ However, in a real system the ions will move and there is therefore a more diffuse layer close to the interface.

The Gouy–Chapman theory leads to an effective electrical double layer which is represented by the decay of the potential ψ_0 as a function of distance from the interface. The potential is assumed to decay approximately exponentially. The thickness of this layer is characterized by the point at which the potential has dropped to $1/e$ of its initial value and is defined by the double layer thickness $1/\kappa$. The value of κ is defined by $\kappa = \sqrt{8\pi e^2 c_0 z^2 / \epsilon kT}$, where e is the electron charge, c_0 the bulk electrolyte concentration, z the valence and ϵ the dielectric constant. The double layer thickness is $\sim 10 \text{ \AA}$ for 10^{-1} M and 100 \AA for 10^{-3} M of a univalent ion combination.

A refined version of the potential due to Stern allows for there to be a contact layer of counter ions that does not exchange rapidly; behind this is a more diffuse layer of charge. The Gouy–Chapman^{5,6} calculations give too high a charge and this is reduced by the adsorbed counter ions (Figure 11.9).

Original calculations based on point charges gave too high an ionic concentration near the surface. The refined calculations introduce a finite ion size into the calculation that allows for the fact that the ions may have a hydration sheath and allows for specific interactions with counter ions. The theory simply splits the potential function into two parts: the compact contact layer where the potential falls quickly from ψ_0 to ψ_1 and a diffuse layer where the potential drops more slowly to zero.

11.11 Particle (Micelle) Stabilization

The stabilization of a micelle can be achieved by two distinctly different mechanisms depending upon whether the molecules involved are able to

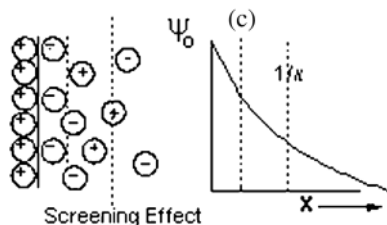


Figure 11.9 Stern potential indicating the contact layer and the diffuse layer profiles.

dissociate into charged species or not. If the stabilizing molecules are able to create ionic species the micelles are able to repel one another and hence there is a barrier that has to be overcome before the size of the particle can be increased to lower the total energy. If the molecules are unable to carry a charge then entropic factors have to provide the stabilization.

11.11.1 Charge Stabilization: Derjaguin–Landau–Verwey–Overbeek (DLVO) Theory

The DLVO theory^{7,8} describes the electrostatic stabilization of charged colloidal particles. The charges on the particles may be associated with ionization of specific groups on the molecules, as in the case of proteins or attributed to charges adsorbed onto a particle or molecule. If two particles carry similar charges, then there will be repulsive interactions between them. The double layers described above, model the charge distribution close to such a surface. Unlike charges lead to attractive interactions which will attempt to cause the particles to merge and if the particles are deformable then they will grow to a single-phase large particle and ultimately separate into two phases. The behaviour of charged colloids is a controlled balance of these two effects.

To demonstrate the principles of the theory, it is useful to simplify the problem and initially consider the interaction between parallel plates. If the particle is large, then the parallel plate model is a good approximation to reality. This theory can then be generalized to include spheres by the introduction of a geometrical averaging factor. The so-called Hamaker potentials allow for this generalization of the interaction potentials. Although the spherical case is considered to be more descriptive of colloids, the mathematics are more difficult and the geometrical factors more difficult to understand. The idealized interaction potential is shown in Figure 11.10 for an increasing attractive potential and reflects the effects of change in temperature. The potential is the sum of an attractive term which acts at long range and is being progressively increased and a repulsive term which acts at short range and is essentially constant. The curves simulate the variation of the potential as a function of temperature. A stable colloidal dispersion is only obtained when a minimum exists in the potential as a function of the distance of separation of the particles x . The particles will have kinetic energy and if the average thermal energy kT is

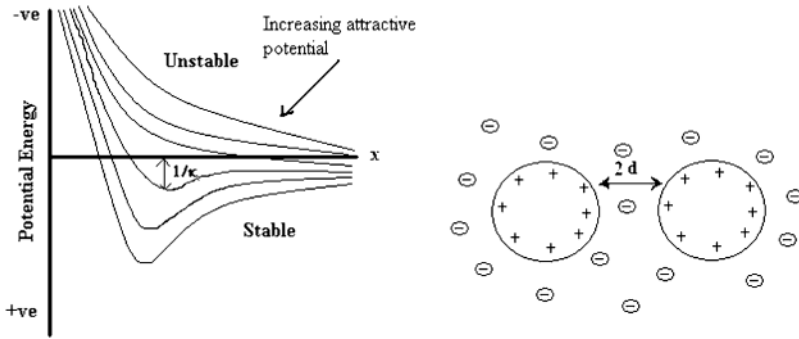


Figure 11.10 Variation of the potential with variation of the strength of the attractive and repulsive contributions to the total potential as a function of particle separation, $2d$.

greater than the stabilization energy depicted as $1/\kappa$, then the particles can move about freely. If the thermal energy is less than kT , then the particles will order at a distance dictated by the location of the minimum energy. The system is able to *self-assemble*.

(i) Repulsive term. The term for two parallel plates held at a distance $2d$ apart and assuming that the double layer has the Gouy–Chapman form:^{5,6}

$$V_{\text{rep}} = \left\{ \frac{64c_0kT}{\kappa} \right\} \gamma^2 \exp(-2\kappa d) \tag{11.21}$$

where $\gamma = \exp(ze\psi_0/2kT) - 1$.

For the Stern model ψ_0 is replaced by ψ_1 , to allow for the effect of contact charges on the shape of the potential.

(ii) Attractive term. Similarly the attractive term has the form

$$V_{\text{att}} = -\frac{A}{48\pi d^2} \tag{11.22}$$

where A is a constant which depends on the density and polarizability of the media. The combination of these two terms gives potential curves of the form shown in Figure 11.10. The balance between the attractive and repulsive forces gives a minimum which is indicative of a stable state. The height of the barrier determines the kinetic stability of the colloid. If $E \gg kT$ then we have kinetic stability; if $E \leq kT$, the system is not stable. The magnitude of κ decreases as the electrolyte concentration decreases and there is a critical value for stability which is determined by $\partial V_{\text{total}}/\partial x = 0$. Hence

$$V_{\text{total}} = V_{\text{repulsive}} + V_{\text{attractive}} = \left\{ 64 \frac{c_0kT}{\kappa} \right\} \gamma^2 \exp(-2\kappa d) - \frac{A}{48\pi d^2} \tag{11.23}$$

Where V_{total} and $\partial V_{\text{total}}/\partial x$ both equal zero, the stabilizing barrier disappears and we get flocculation. Thus

$$dV_{\text{total}}/dx = -2kV_{\text{rep}} - 2V_{\text{att}}/d = 0 \quad (11.24)$$

and

$$\frac{64c_0kT}{\kappa\gamma^2}\exp(-2\kappa d) - \frac{A}{48\pi d^2} = 0 \quad (11.25)$$

For $V_{\text{rep}} + V_{\text{att}} = 0$ and $\kappa d = 1$, eqn (11.25) becomes

$$\frac{64c_0kT}{\kappa\gamma}\exp(-2) = \left(\frac{A}{48\pi}\right)\kappa^2 \quad (11.26)$$

However, $\kappa = (8\pi c_0 e^2 z^6 / \epsilon k T)^{1/2}$ and therefore $c_0 = 107\epsilon^2 k^5 T^5 \gamma^4 / A^2 e^6 z^6$. Inserting reasonable values for a colloidal system in water we obtain $c_0 = 8 \times 10^{-22} (\gamma^4 / A^2 z^6)$ mmol l^{-1} at high potentials $\gamma \rightarrow 1$. The theory predicts flocculation concentration of different electrolytes containing mono-, di- and trivalent counter ions to be in the ratio $1:1/2^6:1/3^6$ or $100:1.6:0.13$.⁸ This theory, in a more generalized form, can be used to describe the behaviour of proteins and other macromolecular species. The theory highlights the extreme sensitivity of the system to the charge stabilization and how change in the charge distribution can destabilize the system (salting out).

11.11.2 Steric or Entropic Stabilization?⁹

Many colloids are dispersed in organic solvents, e.g. carbon black in printing ink, TiO_2 in paints. Many polymer systems, because of the length of the chains involved, form micelle structures as a consequence of *entropic* stabilization. In organic solvents, charging effects are much less pronounced and may be almost absent in relatively low dielectric constant solvents. The polymeric nature of the molecules allows them to create disorder around the particle to which they are attached and act as protective lyophilic colloids. Polymer molecules that can be used in this way have a structure which allows them to be distributed across the interface and will usually have polar and non-polar block segments. In an aqueous system, the polar element will usually be water soluble, whereas the non-polar element will be water insoluble. This difference in solubility will naturally create an interface and the flexibility of the chains dispersed in the water produces the required entropy for entropic stabilization. The approach of a pair of particles and hence their ability to flocculate is inhibited by the extending disordered chains and the overall effect is that of steric stabilization (Figure 11.11). Polymer molecules are sometimes designed to be selectively absorbed onto a specific surface of another polymer particle and ‘wave around’ in the solvent. The waving chain will often have a branched chain structure to inhibit crystallization. This type of stabilizer has the advantage of being less

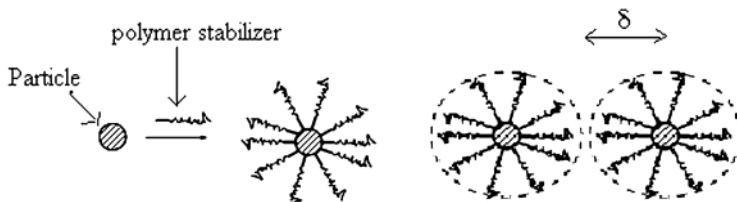


Figure 11.11 Schematic of absorption of a polymer chain on a particle surface and the resultant stabilization. The parameter δ designates the thickness of the disordered layer.

sensitive to pH, electrolyte and temperature changes, and is a vital part of modern non-drip paint systems.

The detailed theoretical modelling of the stabilization process is quite complex; however, a simple model provides the qualitative behaviour of these systems. When two particles approach one another to a distance that is less than 2δ , where δ is the thickness of the adsorbed layer, then the degree of stabilization can be defined in terms of the energy change which occurs upon interaction of the adsorbed layers. The energy term will be a combination of an entropy and enthalpy term: $\Delta G = \Delta H - T\Delta S$. If ΔG is negative, flocculation will occur; if ΔG is positive, then the system will be stabilized.

11.11.3 Entropic Theory

This assumes that adsorbed polymer layers are essentially impenetrable and as the layers approach they become compressed. This compression process will involve a change in configurational entropy, *i.e.* ΔS is negative. The change in the enthalpic interaction is usually neglected so that $\Delta G = -T\Delta S$, ΔG is thus positive and flocculation occurs. The simplest way of considering the polymer is to visualize it as a rod hinged at the surface and of length l (Figure 11.12). If the entropy of an unconstrained polymer chain is described by $S_\infty = k \ln W_\infty$ and that of an constrained system by $S_c = k \ln (W_c)$, then the change in the entropy is $\Delta S = S_c - S_\infty = k \ln (W_c/W_\infty)$.

The number of configurations is proportional to the length of the chain. In the case of the unconstrained molecule this has a value l and in the constrained situation a value h . Then the interaction potential V_r is given by

$$V_r = kT \ln \left(\frac{h}{l} \right) = kT \left(1 - \frac{h}{l} \right) \text{ if } \frac{h}{l} \ll 1$$

If there are n adsorbed molecules in the interface then the total repulsive energy per unit surface area is

$$V_r = N_s kT \theta_\infty \left(1 - \frac{h}{l} \right)$$

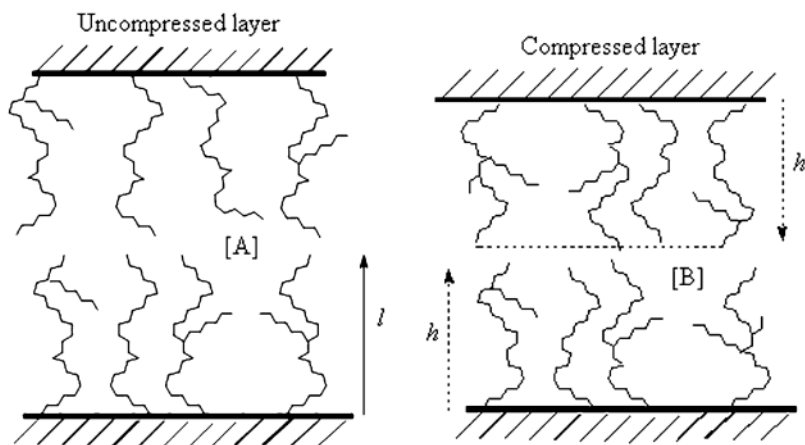


Figure 11.12 Schematic of uncompressed and compressed layers.

where θ_∞ is the fraction of surface covered when the molecules are totally expanded. The theory has been further developed to account for spherical particles of flexible molecules and the effects of the solvent on the configuration. The results are essentially similar except that a shape factor has to be included to allow for the averaging of the potential.

11.12 Phase Behaviour of Micelle Systems¹⁰

As discussed in Chapter 8, a phase separated system has the tendency to form ordered structures. Self-assembly and molecular organization depend on a number of competing factors. Typically there will be differences in the strength of the intramolecular interactions, the flexibility of the chains and the intermolecular forces. The relative magnitude of the attractive hydrophobic forces between hydrophobic tails, the repulsive electrostatic forces between the charged head groups and the head group hydration effects all influence aggregate architecture and stability. From the concepts outlined above in relation to minimization of the surface energy, it is apparent that the curvature of the structure formed is an important criterion for determining the shape. The curvature can be expressed in terms of a dimensionless parameter known as the 'critical packing parameter' v/a_0l_c , where v is the volume of the hydrocarbon chain, assumed to be fluid and incompressible and expressed in terms of the chain length. The chain length l_c is the critical chain length assumed to be approximately equal to l_{\max} , the fully extended chain length. For a molecule containing m chains each with n carbon atoms and having a head group with area a_0 then

$$v = (27.4 + 26.9n)m \quad (11.27)$$

and

$$l_{\max} = 1.5 + 1.265n \quad (11.28)$$

Many surfactants have a molecular structure that involves two long alkane chains being attached to a single polar head group. The double chain structure can significantly influence the packing arrangements. The critical packing parameter can be used as a guide to the aggregate architecture for a given surfactant (Figure 11.13). Typical values and their corresponding aggregate structures are: $v/a_0l_c < 1/3$, spherical micelle; $1/3 < v/a_0l_c < 1/2$, polydispersed cylindrical micelles; $1/2 < v/a_0l_c < 1$, vesicles, oblate micelles or bilayers; $v/a_0l_c > 1$, inverted structures.

As the concentration is increased, the micelles will interact and form a series of regular structures that reflect the detail of the interaction between the species present. This progressive change can be depicted schematically (Figure 11.14). Not all of the phases will be observed, and in the case of micelles, an increase in the temperature will allow the molecules to exceed the stabilization criteria and more open structures can be produced which will eventually flocculate. An idealized surfactant system will usually involve an amphiphilic molecule, a solvent (usually water) and a non-solvent, which may be an oil or other non-polar material. The phase diagram that is obtained is shown in Figure 11.14.

Moving up the water–surfactant axis there is a progressive change in structure. In very dilute solutions, there are isolated surfactant molecules present. Once the CMC has been achieved, micelles will be formed. Increasing the

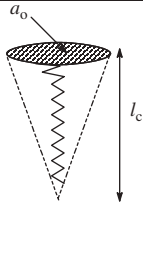
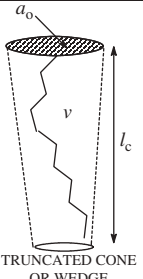
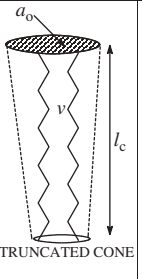
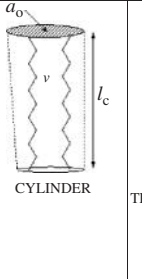
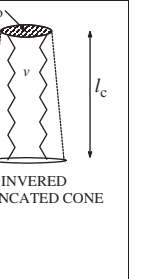


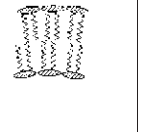
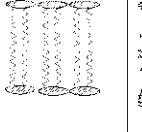
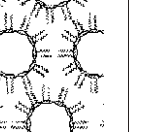
Molecular shape	Single chain with large head group	Single chain with small head group	Double chain with large head group	Double chain with small head group	Double chain having small head group
Critical packing parameter	$< 1/3$	$1/3 - 1/2$	$1/2 - 1$	~ 1	> 1
Critical packing shape					
Structures					
	Spherical micelle	Cylindrical Micelle	Flexible bilayer	Planar bilayer	Inverted micelle

Figure 11.13 Influence of critical packing factors on aggregated structures.

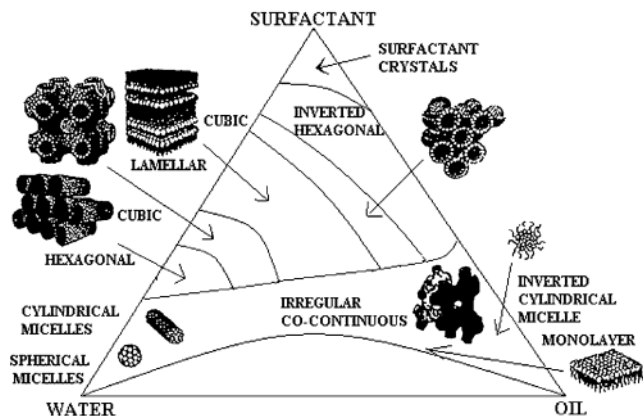


Figure 11.14 Idealized phase diagram for a surfactant–water–oil system.

concentration of surfactant will change the structure of the micelle from a spherical to a cylindrical structure. The first major phase change is between the cylindrical micelles and a hexagonal close packed structure. Subsequent phase changes involve the hexagonal phase changing to a cubic structure and then to a lamellar structure. These are all soft solids and have properties that reflect ever stronger interactions and a progressive change to a hard crystalline state. These intermediate phases will resemble soaps or thick greases. Further increase in concentration causes changes to a cubic phase and then an inverted hexagonal structure and ultimately a crystalline phase is formed if the temperature is below the melt temperature. Moving down the surfactant–oil axis, a simpler set of phase changes is observed which reflect the greater hydrocarbon chain solubility in the oil phase. The phases are therefore the inverse of those in the water–surfactant system and in dilute solution will form inverse micelles. The centre of the phase diagram is the result of the balance of these forces leading to a complex array of phases. Around the centre of the diagram there is a region where the two-phase structures are almost in equilibrium and a co-continuous phase is observed. At low surfactant levels monolayers can be formed at the surface and these will be able to incorporate a small amount of the oil in monolayer. This type of idealized phase diagram is observed for many systems.

11.13 Phase Structures in Polymer Systems

11.13.1 Block Copolymers and Associated Phase Diagrams

Many amphiphilic block copolymers and related oligomeric materials exhibit structure formation at a nanometre scale. By careful selection of the solvent, phase separation can be achieved allowing one block to be dissolved and the other to be immiscible. The head group(s) of a surfactant or the hydrophilic

block(s) of a block copolymer will readily dissolve in water and a poor solvent or non-solvent for the other part of the molecule (e.g. the organic tail(s) of the surfactant or the hydrophobic block(s) of the block copolymer) will self-segregate or disperse in a hydrocarbon phase. This approach leads to the production of micelles, microemulsions, vesicles, monolayers (on surfaces) and many biologically important systems (e.g. cell membranes). In the case of polymeric materials, the number of polymer chains in one micelle is approximately the same and results in the micelle size distributions being very narrow. For polydisperse block copolymers or surfactants, it is found that to minimize the free energy the aggregates formed are of uniform size. The features that are created at the surface of a blend (Chapter 10) are all of similar size and support this contention. The size of the micellar core is determined by the association number and volume of other solvent-phobic species incorporated into the core. Larger micelles can be produced if the core is filled with species that are solvent-phobic. For triblock copolymers with two end blocks in a poor or non-solvent, supramolecular formation with open structures that tend to obey an open-association mechanism can occur¹¹⁻¹³ (Figure 11.15).

The solubility of block copolymers decreases with increasing temperature and above a certain temperature, phase separation occurs, the 'cloud point' is observed.¹³ At higher polymer concentrations, the entanglement of the polymer chains in solution leads to the formation of homogeneous, immobile, gel-like structures. The first gel-like structure is usually a cubic structure (body-centred cubic (bcc) or face-centred cubic (fcc)), formed by an ordered packing of spherical micelles. At even higher polymer concentrations, the arrangement of the hydrophilic and hydrophobic regions leads to the formation of hexagonal

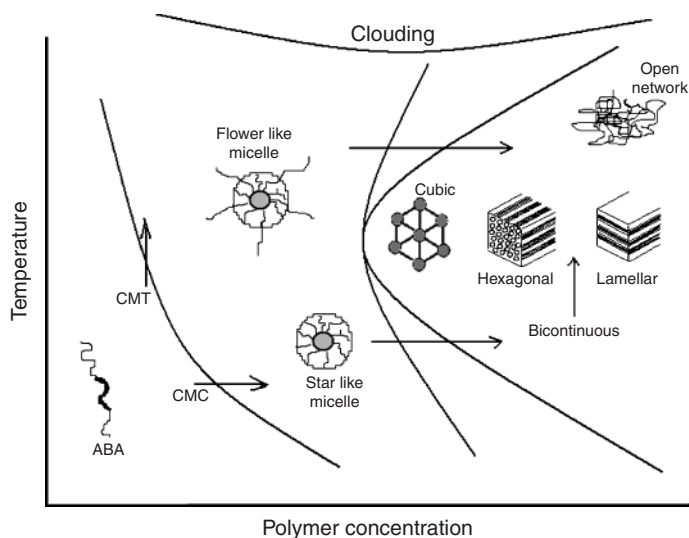


Figure 11.15 Schematic phase diagram for the phase behaviour of amphiphilic block copolymers represented by ABA-type triblock copolymers in aqueous solution.

or lamellar structures. Bicontinuous cubic structure could also be observed between the hexagonal and lamellar regions.^{14–16} For the flower-like micelles formed by a block copolymer in a selective solvent for the middle block, an open network without any ordered structure is generally obtained at high polymer concentrations. Copolymer–water–oil ternary phase diagrams can be much more complicated even at a constant temperature.^{17–23}

Under these conditions, broad distributions of the micellar size and mass can be observed. Furthermore, as a function of external conditions such as temperature or solvent composition, micellar shapes other than spherical can be observed, e.g. prolate^{24–27} or oblate²⁸ ellipsoids of revolution.

11.13.2 Pluronics

One of the most extensively investigated nonionic block copolymer–solvent systems are the Pluronics. This generic name describes a series of triblock copolymers containing hydrophilic A blocks and hydrophobic B blocks or groups, with A and B being polyoxyethylene, polyoxypropylene and polyoxybutylene. The blocks are all polyethers, but the different structure of the alkyl component varies the degree of hydrophilicity of the block, polyoxyethylene being the most hydrophilic and polyoxybutylene being the least hydrophilic to water. The phase behaviour is usually studied with the addition of a non-polar organic solvent, such as xylene. The phase structure has been studied extensively using small-angle X-ray scattering.

The phase behaviour of Pluronics in the presence of water and xylene has been extensively studied.^{21–23} The ternary phase diagram of Pluronic P84 (E19P44E19)/water/*p*-xylene studied by Alexandridis *et al.*²³ at room temperature is reproduced in Figure 11.16. The various phases identified are similar to those for the idealized surfactant system (Figure 11.14). At least nine different phases have been identified: normal micellar solution (oil-in-water), cubic, hexagonal, bicontinuous cubic, reversed micellar solution (water-in-oil), cubic, hexagonal, bicontinuous cubic and lamellar phases. These nine phase classes represent all known possible phases in such a ternary system. In general, block copolymer systems can offer various different nanoscale templates such as three-dimensional (3D) cubic packings of spherical units, two-dimensional (2D) hexagonal packings of cylindrical units, one-dimensional (1D) periodic lamellar systems and 3D bicontinuous cubic morphologies. Considering that the total chain length, the block length ratio, the chain architecture and the chemical composition of block copolymers are all adjustable, the templates can be easily tuned to fit specific requirements. Sometimes, micelles with differing morphologies (e.g. ellipsoids or rods) can also be achieved by choosing a suitable combination of block length and solvent quality. Therefore, it is not surprising that block copolymers have been much applied in nanofabrication processes.

The changes in the phase structure can have dramatic effects on the physical properties, and some of the phases are essentially soft solids rather than being liquids. The very rich structures of polymer matrices and the subsequent formation of nanostructured materials often require an extensive range of

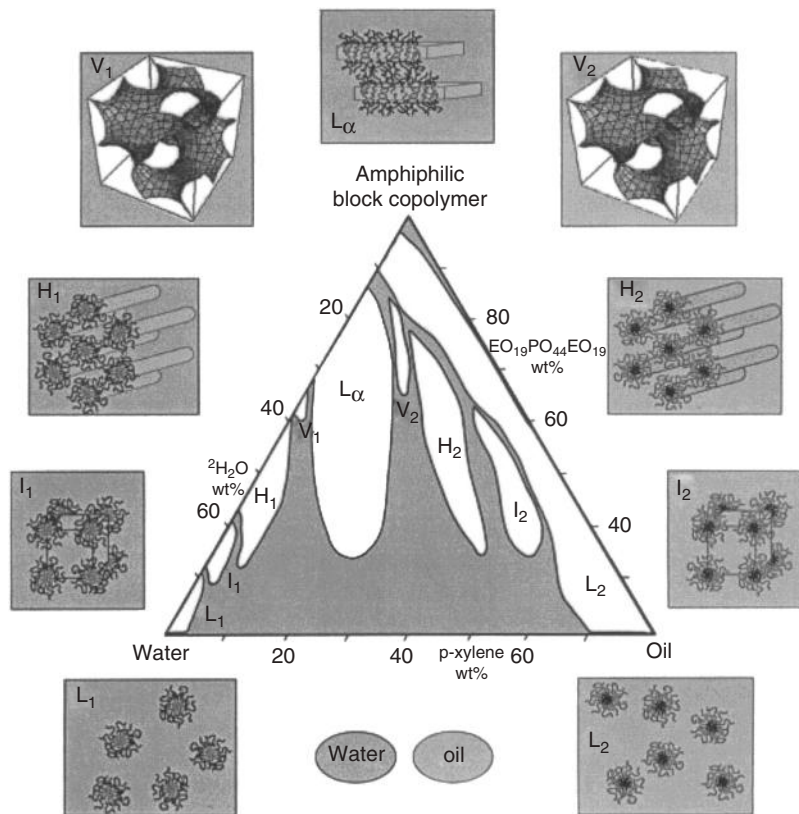


Figure 11.16 Ternary phase diagram of Pluronic P84 (E19P44E19)/water/*p*-xylene at room temperature. Nine different phases can be identified: normal (oil-in-water) micellar solution L1, cubic I1, hexagonal H1, bicontinuous cubic V1, reversed (water-in-oil) micellar solution L2, cubic I2, hexagonal H2, bicontinuous cubic V2 and lamellar phases.²³

physical techniques to characterize the complex structures over a range of length. It is apparent that with charged polymer systems and also those capable of entropic stabilization, pre-assembly can occur in the fluid phase prior to forming a solid, and this is an important mechanism for the creation of structure in the solid state. Biological systems use this mechanism to great advantage and create complex structures which are capable of executing at a molecular level a specific physical function. This pre-assembly process is able to create a number of the higher order structures that are discussed in Chapter 12.

Recommended Reading

A.W. Adamson and A.P. Gast, *Physical Chemistry of Surfaces*, Wiley Interscience, New York, 1997.

S.Friberg, *Lyotropic Liquid Crystals*, Advances in Chemistry Series 152, American Chemical Society, Washington, DC, 1976.

R.J. Hunter, *Foundations of Colloid Science*, Oxford University Press, 2002.

S. Ross and I.D. Morrison, *Colloidal Systems and Interfaces*, John Wiley, New York, 1988.

References

1. S. Ross and I.D. Morrison, *Colloidal Systems and Interfaces*, John Wiley, New York, 1988.
2. R.J. Hunter, *Foundations of Colloid Science*, Oxford University Press, 2002.
3. A.W. Adamson and A.P. Gast, *Physical Chemistry of Surfaces*, Wiley Interscience, New York, 1997.
4. D.A. Cadenhead, *Ind. Eng. Chem.*, 1969, **61**(4), 22.
5. G. Gouy, *J. Phys. Theor. Appl.*, 1910, **9**(4), 457.
6. D.L.A. Chapman, *Philos. Mag.*, 1913, **25**(6), 475.
7. B.V. Derjaguin and L. Landau, *Acta Physicochem. USSR*, 1941, **14**, 733.
8. H. Koelmans and J. Overbeck, *Discuss. Faraday Soc.*, 1954, **18**, 52.
9. D.H. Napper, *Polymeric Stabilization of Colloidal Dispersions*, Academic Press, London, 1983.
10. R.M. Pashley and M.E. Karaman, *Applied Colloid and Surface Chemistry*, John Wiley, Chichester, UK, 2004, p. 74.
11. T. Liu, Z.K. Zhou, C.H. Wu, B. Chu, D.K. Schneider and V.M. Nace, *J. Phys. Chem. B*, 1997, **101**(43), 8808.
12. T. Liu, L.-Z. Liu and B. Chu, in *Block Copolymers: Self-Assembly and Applications*, ed. P. Alexandridis and B. Lindman, Elsevier, Amsterdam, 2000.
13. T. Liu, V.M. Nace and B. Chu, *J. Phys. Chem. B*, 1997, **101**(41), 8074.
14. Z. Tuzar and P. Kratochvil, in *Surface and Colloid Science*, ed. E. Matijevic, Plenum Press, New York, 1993, vol. 15.
15. K. Kon-no, in *Surface and Colloid Science*, ed. E. Matijevic, Plenum Press, New York, 1993, vol. 15.
16. B. Chu and Z. Zhou, in *Nonionic Surfactants*, ed. V.M. Nace, Marcel Dekker, New York, 1996.
17. K. Mortensen, W. Brown and E. Jorgensen, *Macromolecules*, 1994, **27**(20), 5654.
18. G. Wanka, H. Hoffmann and W. Ulbricht, *Colloid Polym. Sci.*, 1990, **268**(2), 101.
19. K. Mortensen, W. Brown and B. Norden, *Phys. Rev. Lett.*, 1992, **68**(15), 2343.
20. P. Alexandridis and K. Andersson, *J. Phys. Chem. B*, 1997, **101**(41), 8103.
21. P. Holmqvist, P. Alexandridis and B. Lindman, *Macromolecules*, 1997, **30**(22), 6788.
22. P. Alexandridis, U. Olsson and B. Lindman, *Langmuir*, 1996, **12**(6), 1419.

23. P. Alexandridis, U. Olsson and B. Lindman, *Langmuir*, 1998, **14**(10), 2627.
24. H. Utiyama, K. Takenaka, M. Mizumori, M. Fukuda, Y. Tsunashi and M. Kurata, *Macromolecules*, 1974, **7**(4), 515.
25. M. Antonietti, S. Heinz, M. Schmidt and C. Rosenauer, *Macromolecules*, 1994, **27**(12), 3276.
26. V. Castelletto, R. Itri and L. Q. Amaral, *J. Chem. Phys.*, 1997, **107**(2), 638.
27. M. Leaver, V. Rajagopalan, O. Ulf and K. Mortensen, *Phys. Chem. Chem. Phys.*, 2000, **2**(13), 2951.
28. G. W. Wu, Z. K. Zhou and B. Chu, *J. Polym. Sci., Part B: Polym. Phys.*, 1993, **31**(13), 2035.

CHAPTER 12

Molecular Organization and Higher Order Structures

12.1 Introduction

In the previous chapters, the organization of polymers and small molecules has been studied at macroscopic, microscopic and molecular level. In many of the systems the structures observed scale relatively simply from the molecular to the macroscopic structure. In the case of a system such as polyethylene, the type of organization observed depends on the scale of the structure being examined. At the nanometre level folding of the chains produces lamellar structures. Because these lamellae are nucleated at the same instant at various points in the crystallizing volume the growing nuclei and/or clusters of lamellae interact and spherulitic structures are observed. Between these spherulites are grain boundaries and these are the dominant feature at the micrometre level. At macroscopic level all these features are not observed and the material appears smooth and homogeneous. Understanding the macroscopic behaviour requires a knowledge as to how these different levels of morphology interact. In biological systems, nature self-assembles complex structures from relatively simple components. Nature recognizes the way in which molecular order scales from molecular to macrostructure, acknowledges the advantages of the occurrence of composite structure in a material and demonstrates the way in which nature builds in rigidity, flexibility and ductility into polymeric materials. It is impossible to cover all natural materials in a book of this size and we will look at only three examples of such systems to illustrate the parallels between natural and synthetic materials.

12.2 Hair

The structure of hair can be considered schematically as in Figure 12.1.

The primary core molecular structure is represented in terms of the α -helix of keratin, which is a major constituent of hair. Keratins are the most abundant proteins and are the main component of the horny layer of epidermis and the

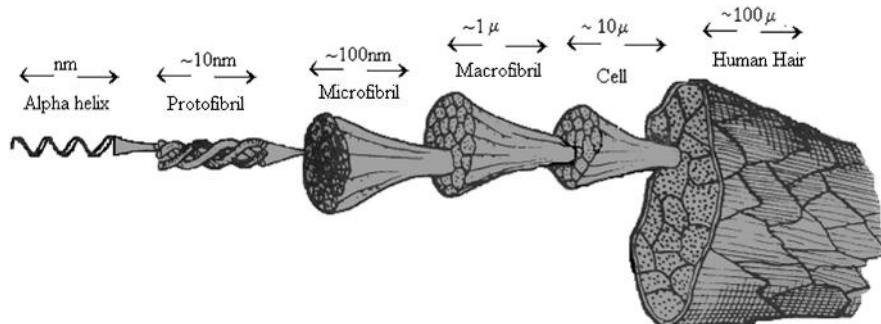
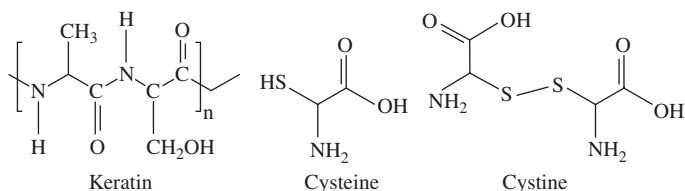


Figure 12.1 Schematic of human hair showing level of morphology.

appendages such as hair, nails, scales, quills, horns and feathers. Keratinous tissues provide strong mechanical support and a chemical barrier. The hard α -keratinous tissue occurs in quills and hair and forms well-ordered and oriented supramolecular architectures. Hair contains protofibrils which are made up of keratin combined with other proteins. The protofibrils in turn cluster to form a microfibril that in turn forms part of a macrofibril that are the main part of the cell structure. Hair is constituted from a series of cells. The platelets on the surface of the hair are hydrophobic, whereas the core material is hydrophilic. The principal difference between various forms of hair lies in the nature and cysteine/cystine content of these proteins that are part of the cell walls and are incorporated in the microfibrils. The protein plays the role of a *habit* modifier and controls the organization of the keratin from the initially formed amorphous phase to an organized crystalline structure.



The chemical structure is in fact much more complex than implied by this simple description, but it illustrates the hierarchy of levels of organization that are present within the hair.¹⁻⁵ Pigmentation and the detailed balance of various proteins impact on the colour, structure and texture. Micro X-ray analysis of hair has shown the existence of two major polymorph intermediate filament (IF) architectures. Just outside of the follicle, the filaments are characterized by a diameter of 100 Å and have a low core density. As the hair grows, lateral aggregation of the filaments occurs into a more compact network of filaments and there is a contraction of their diameter to ~ 75 Å and associated long-range longitudinal ordering of the microfibril. The architecture of the IF in the upper zones is specific to hard α -keratin, whilst other architectures are found in the lower zone.¹ Examination of the structure at high resolution indicates that two

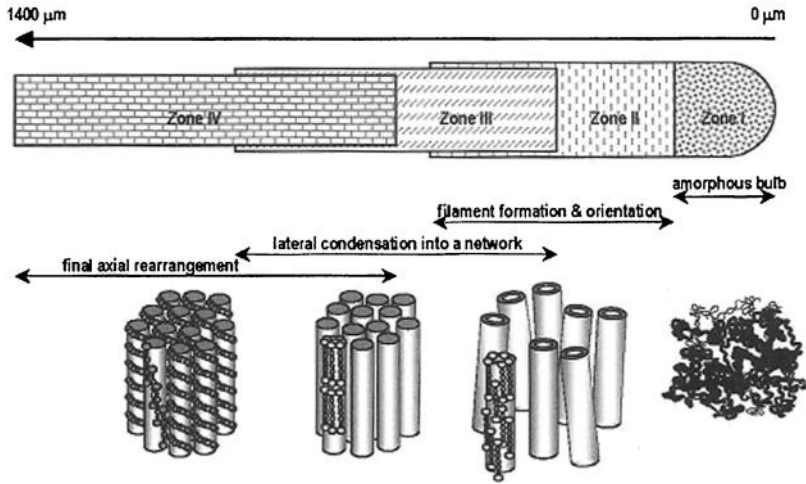


Figure 12.2 Schematic of the changes in morphology as a hair grows.

~ 450 Å long keratin chains are assembled into a dimeric molecule with a rod-like character and these form the α -helical coils. These dimeric molecules are assembled, both longitudinally and laterally, forming long cylinder-shaped filaments with an axial well-defined periodic ordering. The number of chains across a filament is ~ 32 chains. These polymorphic changes give hair its strength and the process can be represented schematically as in Figure 12.2.

Water can plasticize hair by interaction with the core of the cell but loses the water when dried. The outer structure contains cystine that has a disulfide linkage and these crosslinks are important in determining the overall organization of the chains within the hair structure and control the detailed morphology that can be adopted. Differences between hair types are reflected in different distributions of the keratin chains, the nature and distribution of the proteins and the type and distribution of the pigment. The proteins, in this case, are playing an important role in the control of the formation of the crystal structure within the core fibres.

12.3 Structure in Cellulose Fibres²⁻⁶

A classic example of the creation of macrostructure from molecular organization is cellulose-based fibre materials. Cellulose is the dominant polysaccharide in plant cell walls and is often touted as being the most abundant biopolymer on earth. A basic cellulose unit, known as the elementary fibril, contains thirty-six 1,4- β -D-linked polyanhydroglucopyranose chains⁷ (Figure 12.3a), and may eventually be coated with non-cellulosic polysaccharides to form the cell wall microfibril. These microfibrils are then crosslinked by hemicelluloses/pectin matrixes during cell growth. The cellulose molecule is constrained to adopt

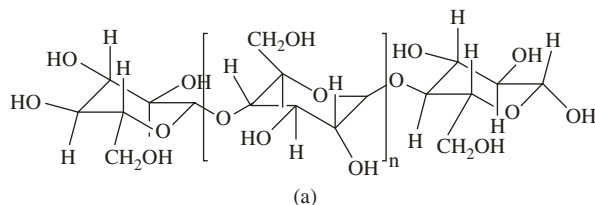


Figure 12.3 Composition and conformation of the cellulose molecule.

certain conformations by various intra- and intermolecular hydrogen bondings which are created when the polymer chains are brought close to one another (Figure 12.3b).

Close inspection of the relative orientation of the rings indicates that the pendant hydroxyl groups can interact to give a lower energy structure if the bridge ether is slightly twisted. As a consequence the backbone of the cellulose chain forms a helical structure with a pitch of 12 rings per rotation. In this respect there are similarities with the keratin helical structure in hair. As with the case of hair, these microfibrils are then themselves organized to form the overall fibre structure (Figure 12.4). Transmission electron microscopy (TEM) of the cell wall indicates that microfibrils have a diameter of between 2 and 10 nm. In native *Valonia* cellulose crystal the packing appears to be hexagonal with dimensions of 2–3 nm.

To understand the physical properties of cellulose, it is appropriate to consider organization at three different levels.¹⁰

1. *The molecular level.* Cellulose as a consequence of the favoured hydrogen bonding interactions adopts an extended rod-like form which aids packing into crystalline structures. Molecular modeling⁴ has allowed the development of a detailed knowledge of the conformational preferences of polymeric systems and realistic models of the chain backbone structure to be created. The local structure of the chain is assumed to involve the β -D-glucose existing in the pyranose form and the ring adopts a 4C_1 chair formation, which is the lowest energy conformation for β -D-glucopyranose. The presence of intramolecular

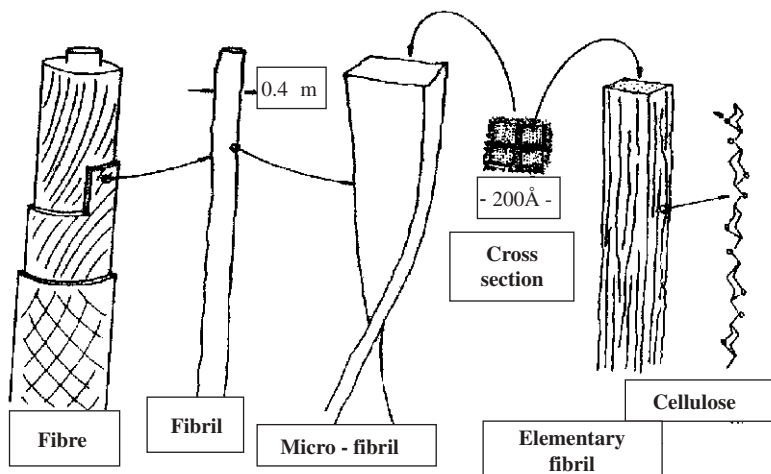


Figure 12.4 Morphology of a cellulose fibre.⁸⁻¹⁰

hydrogen bonding between the hydroxyl group in the 3 position and the ring ether oxygen in the 5 position imposes a twist on the C(1)–O(1) and the C(4)–O(4) glucosidic bonds which results in the chain adopting a helical conformation. Varying how the rigid chains pack together leads to the possibility of polymorphic forms being obtained.^{8,9} The study of these structures has been the subject of active research for many years and reflects the fact that nature can control the way in which the chains organize into the larger structures that ultimately generate the variety of physical properties that make these materials useful. For instance, cotton fibres in the bud form are known to exist in a disordered structure and rapidly form the cellulose I structure when the bud opens. Cellulose I structure is a thermodynamically a metastable crystalline structure, which on dissolution in a suitable solvent is not re-formed when the polymer is reprecipitated.

2. The supermolecular level. The individual chains are aggregated into polymorphs that form microcrystallites and fibrils. The packing of the cellulose molecules in these hydrogen bonded systems is very dense and none of the hydroxyls in the interior of the crystal are easily accessible. The ability to exchange hydrogen has been explored by investigation of the change in the infrared spectra when cellulose is suspended in deuterium oxide. Native cellulose exhibits the cellulose I structure.^{7,8} The mercerized or regenerated cellulose exhibits different structure designated cellulose II. The latter is considered the more thermodynamically stable of the two forms and the nature of the hydroxyl group interactions is different in the two forms. The average hydrogen bond length in the case of cellulose I is 2.72×10^{-10} m which is markedly shorter than the value of 2.80×10^{-10} m in cellulose II. The more dense structure and greater involvement of hydrogen bonding are reflected in the

lower susceptibility to reaction of the regenerated cellulose with the cellulose II structure. Besides the cellulose I and cellulose II polymorphic lattice structures, there are cellulose III and cellulose IV crystal modifications. The cellulose III structure is formed when the reaction product of native cellulose fibres with liquid ammonia is decomposed and closely resembles the cellulose II structure. The cellulose IV structure is obtained by treatment of regenerated cellulose fibres in a hot bath under conditions of the fibres being stretched. The degree of order inside and around these fibrils and their perfection of orientation with respect to the fibre axis are all variables that require to be characterized. A variety of different methods have been used to examine the 'crystalline/amorphous' ratio and the accessibility of the crystalline regions. Among the methods that have been used are the initial loss of matter in hydrolysis, heterogeneous oxidation, deuterium exchange studies, formic acid esterification, hydrogen evolution from the reaction of metallic sodium with cellulose, water and nitrogen adsorption, density measurements, X-ray diffraction and infrared spectroscopy to name just a few. The microstructure of the cell walls is readily visualized using atomic force microscopy (AFM) (Figure 12.5).

The space between the cellulose fibres is filled with hemicellulose, the form of the structure and composition of which varies from plant to plant:

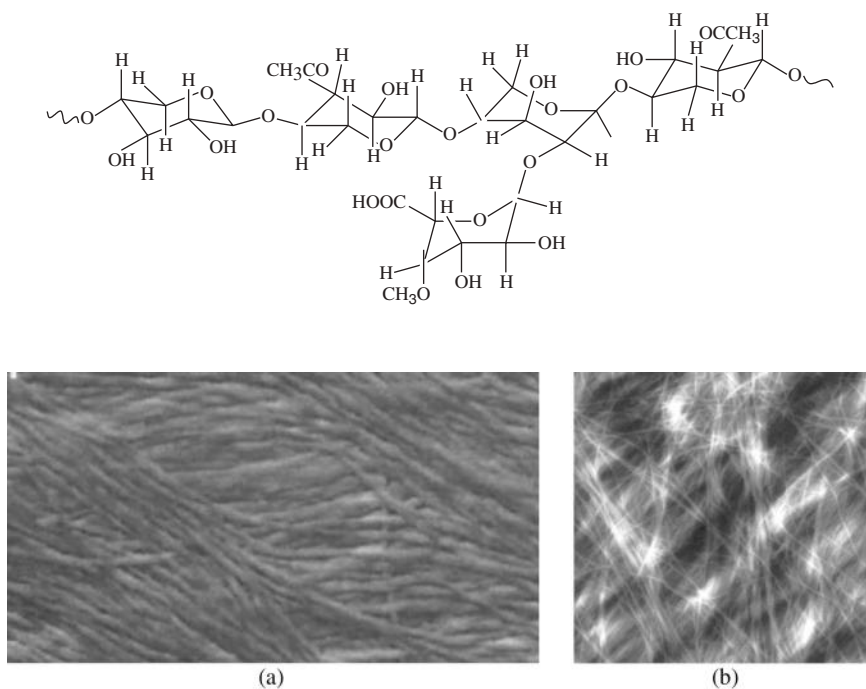
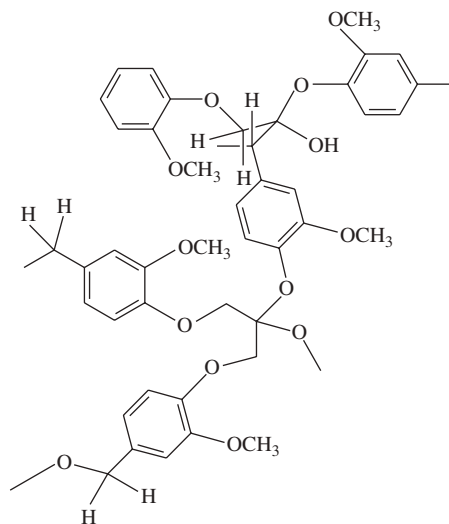


Figure 12.5 AFM images of (a) microfibrils coated with non-cellulosic polymer and (b) the primary wall structure showing microfibrils aligned parallel to one another and the macrofibrils.²

and *lignins* which are complex aromatic-containing hydrocarbon polymers:



Lignin

Both the hemicellulose and lignin structures are representative indicating that unlike cellulose they are unable to form the well-ordered and ultimately crystalline structure which gives these materials their useful properties.

3. *The morphological level.* The fibrillar crystalline strands are in turn organized into the ‘cross-morphology’ of the fibre, the existence of native cell wall layers of the skin–core structure in synthetic fibres, the presence of interfibrillar interstices and voids, *etc.* In particular, the primary wall and outer layer of the secondary wall (S1) in which the fibrils are laid down in a criss-cross fashioned helical manner strongly affect the swelling behaviour and the physical and chemical properties. The increase in tensile strength of cotton fibres on wetting and liquid ammonia treatments could be traced to the hindrance of lateral swelling and the swelling compression exerted on the fibrils in the inner secondary wall layers.

The scale of the organization can be visualized; the fibre structures require to be examined at different levels of magnification^{5–8} (Figure 12.6). The physical and chemical properties of the cellulose fibre are mainly affected by:

- The constitution of the cellulose molecule: the presence of the 1,4-glycoside linkages between glucose units, the three reactive hydroxyls and their involvement in intra- and intermolecular hydrogen bonding which leads to the twisted helical structure.
- The length of the cellulose molecules, especially its relation to the length of the elementary crystals or fused fibrillar aggregations. Recent studies favour the idea that the cellulosic material is dispersed in a matrix of non-cellulosic material. The ordered cellulosic fibres are organized in a pseudo-liquid crystalline form.^{2–6} This type of model is consistent with many physical properties of these materials (Figure 12.6b).

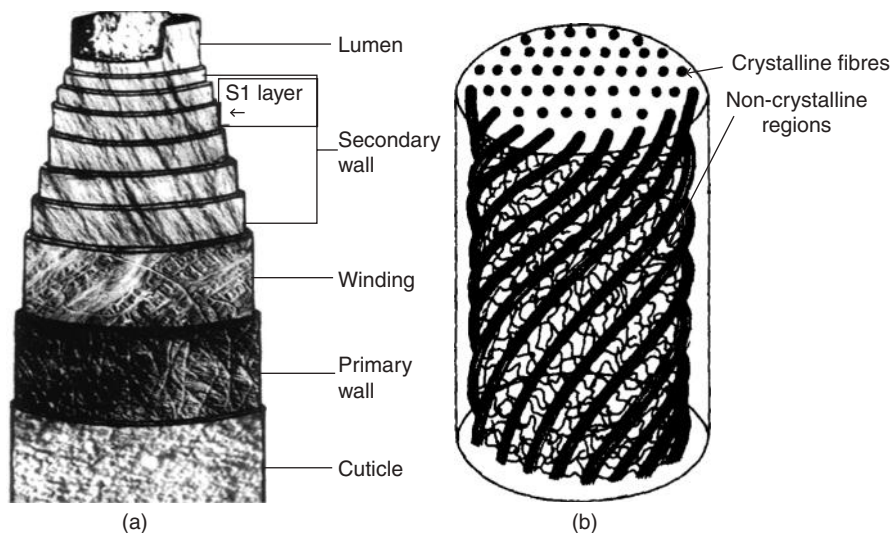


Figure 12.6 (a) Schematic of the various levels of morphology to be found in a cotton linters fibre. (b) Model of fibre structure based on rigid fibres in an amorphous matrix.⁴

- The criss-cross dimensions in the well-ordered fibrillar elements.
- The accessible surface of the fibrils or their aggregations in relation to the fibrillar dimensions.
- The accessible regions interlinking the crystallites in the elementary fibrils.
- The presence of interfibrillar interstices, voids and capillaries and their relationship to the degree of orientation of the fibrillar elements with respect to the fibre axis.

In the case of cotton and other cellulose-based systems, the structure is influenced by the outer layer around the fibre (cuticle) that is composed mainly of hemicellulose. The role of these hemicellulose polymers is critical in the determination of the macroscopic physical properties of the fibre. The winding wall plays an important role in retaining the rigidity of the structure and the layered criss-cross structure will immediately be recognized by engineers as an important element of composite design, allowing extensibility, flexibility and load-bearing properties to be achieved in the same structure. The lumen is a hollow section that runs the length of the fibre and imparts high impact properties as well as allowing the rapid loss of moisture which occurs when the linters emerges from the cotton bud.

The detailed texture of the fibre has been a point of some recent discussion.¹⁴ The cell wall textures are known as axial, transverse, crossed helicoidal and random (Figure 12.7).

Other types of texture are derived from these basic types by the successive deposition of different textures as shown in Figure 12.6. In elongating plants,

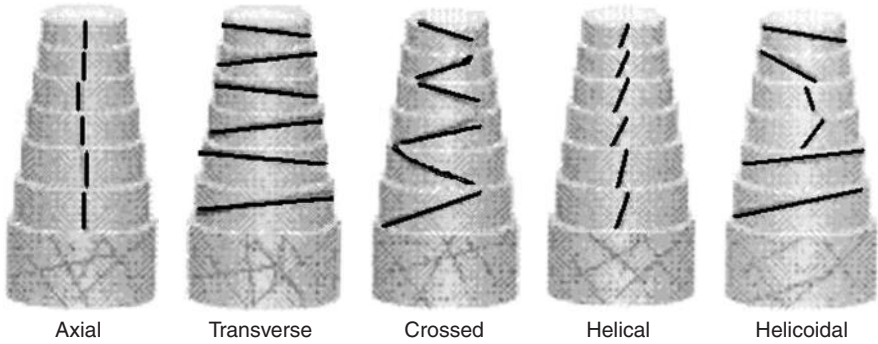


Figure 12.7 Schematic of the typical fibre orientations found in cell walls. Bold lines indicate the fibre alignment.

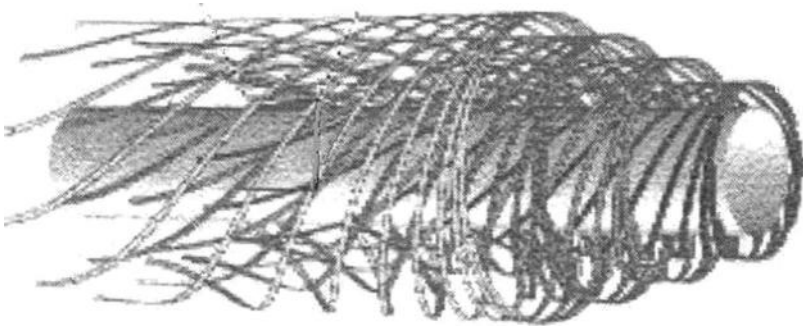


Figure 12.8 Visualization of the geometry development for long fibres.¹⁴

the cortical microtubules as well as the cellulose microfibrils that are being deposited are both transverse to the elongation direction of the cells. Scientists faced with helicoidal cell walls in which microtubes and the cellulose microfibrils did not match realized that the helicoidal walls resemble cholesteric liquid crystals that are known to self-assemble spontaneously. However, this type of equilibrium assembly can only take place when there is sufficient bulk material present. It has been proposed¹⁴ that since cellulose microfibrils are long slender structures the angle that the fibres adopt relative to the axis is dictated by the number of tapes (N), their width (w) and the cell diameter (D). The angle is defined by

$$\sin \alpha = \frac{Nw}{\pi D} \quad (12.1)$$

The number of tapes is dictated by the number of active synthetic sites in the membrane. In an *E. hyemale* root hair membrane this distance between the tapes is ~ 150 nm. This model allows the generation of a number of different

textures observed in plants. A visualization of the fibre forming around the central core is shown in Figure 12.8.

12.4 Natural Silks¹⁴

Natural silk is the archetypal supramolecular assembly of polymer fibres.¹⁴ Silk is produced by *Bombyx mori* silk worms and spiders and is generated from protein molecules that are able to aggregate into a strong fibre. Spiders produce several different types of silk, covering a wide range of properties and applications. The golden orb weaver (*Nephila clavipes*) secretes from the major ampullate glands a dragline, which forms the radial threads of the web as well as providing a 'safety rope' that the spider can rely on if it falls. The fibres have a high tensile strength and modulus and strain to failure. In contrast, the capture thread (viscid silk) produced by the flagelliform glands is highly compliant and able to absorb the kinetic energy of captured flying insects. Other silks spun by the spider are used for swathing prey and are tough and resistant to chemical or photochemical degradation.

12.4.1 Silk Fibre Chemistry

Each form of silk is slightly different. In the case of *Nephila clavipes*, DNA analysis suggests the existence of two similar proteins of molar mass 320 kDa in the silk produced by the spider. Spidroin 1 is characterized by short runs (5–7 residues) of polyalanine separated by approximately five repeat units of a Gly-Gly-X motif, where X is principally one of the large side-chain amino acids Gln, Tyr and Leu. Spidroin 2 has a slightly longer run of polyalanine (6–10 residues) and also contains several proline-containing pentapeptides that include Gly-Tyr-Gly-Pro-Gly, Gly-Pro-Gly-Gly-Tyr and Gly-Pro-Gly-Gln-Gln. The proline content of spidroin 2 precludes its forming regular, crystallizable conformations. Spidroins 1 and 2, respectively, are 719 and 628 residues long, each including a 'tail' that is slightly more hydrophilic. These C-terminal regions contain approximately 60 residues and no repeating motif is apparent. The complex and imperfectly repeating monomer sequence has several significant consequences for fibre processing, microstructural assembly and product properties.

12.4.2 Silk Fibre Processing

The DNA of silk fibre is synthesized in aqueous solution in the spinneret and at this stage is amorphous. It is forced out through an orifice in a process that is rather akin to polymer extrusion into air. The spider using its legs to draw silk through the spinnerets may augment this spinning process. Within the spinnerets, the 30 wt% aqueous solution of the protein is a high-viscosity fluid. The spinning process involves formation of a lower viscosity, shear-sensitive liquid crystalline phase as protein concentration is increased by evaporation of water.

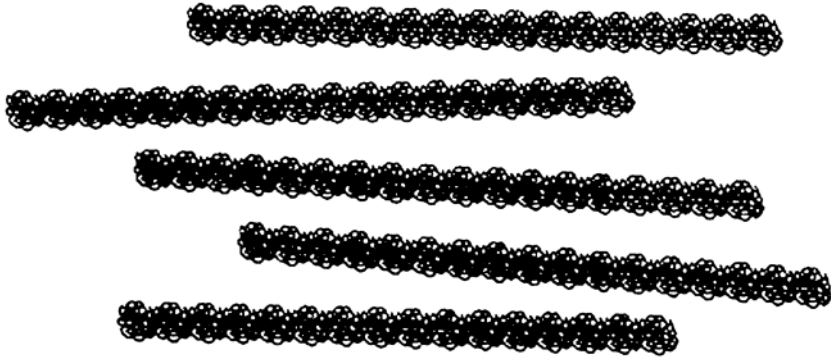


Figure 12.9 Model of liquid crystalline domain in silk secretion.¹⁴

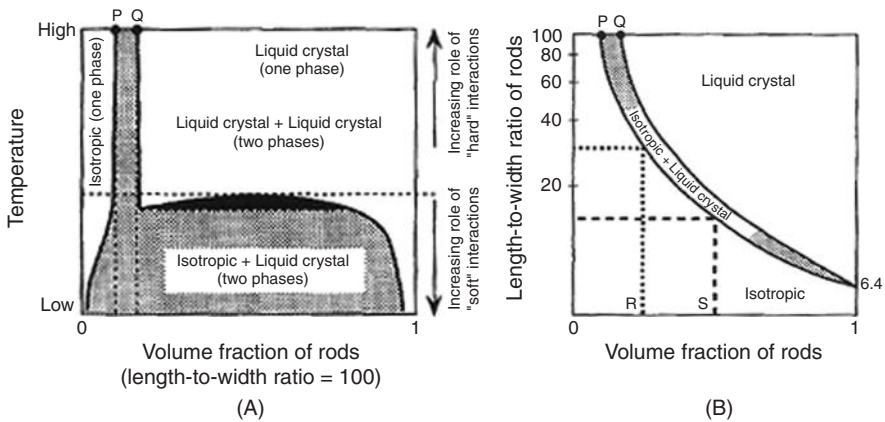


Figure 12.10 Liquid crystal phase formation by rods (length: diameter = 108 : 1): prediction of a simple lattice model.¹⁴

The lowering of the viscosity is associated with the formation of supramolecular rod-like structures created by aggregation of the solubilized protein chains. Figure 12.9 shows a simple model of isotropic fibroin coils, dissolved in water and arranged into orientationally ordered supramolecular rods.

This simple model accommodates the existence of rod-like structures needed for liquid crystal formation, without recourse to anisotropy of individual molecules. The secretions are biphasic (mixed isotropic/liquid crystalline) over a narrow concentration range implying that they have the thermodynamic characteristics typical of an athermal liquid crystalline solution (Figure 12.10).

The molecules must have a rigid rod structure that can align and have a rod axial ratio with an upper limit of around 30, since the biphasic regime starts at a concentration greater than approximately 30 wt%. The concentration of protein in the extruded fibre is ~24%, typical of natural silk secretion prior to drying, and the rod axial ratio has a lower limit greater than the minimum

value needed to sustain liquid crystallinity, ~ 6.4 . The theoretical prediction of the phase diagram for an assembly of rods (Figure 12.10a) shows the athermal behaviour when the solvent–rod interactions cause the biphasic region of the phase diagram to form a ‘chimney’ that spans only a narrow range of concentrations. The concentration range covered by the ‘chimney’ depends on the length-to-diameter ratio of the rods (Figure 12.10b). The concentration at R is 24 vol.%, corresponding to the value typical of silk secretion stored in the gland, suggesting a maximum rod length-to-diameter ratio of approximately 30. The concentration at S is a 50 vol.% solution and is associated with the maximum predicted from birefringence and occurs with a rod length-to-diameter ratio of ~ 15 , in agreement with experiment.

12.4.3 Silk Fibre Microstructures

The strong, stiff, tough fibre microstructure is created by processing the liquid crystalline fluids that are denatured as a consequence of the shear process. The fibre microstructure is composed of ordered regions of varying size and degree of internal perfection. The packing of these entities can be described in terms of interaction between sequences that consist of crystallizable polyalanine and are disrupted by the GGX motifs. The effect of shear is to create a metastable, β -strand conformation. The resultant structure is composed of ordered regions ~ 20 Å across of pure polyalanine that are distributed throughout the matrix, and characterized by a uniform intersheet spacing. At the other end of the size spectrum, there are imperfectly ordered regions of mixed (polyalanine and GGX) composition that are a few hundred nanometres across; internally, their composition varies on the approximate scale of the dominant motif lengths, a few nanometres, which in turn leads to variations in the local intersheet spacing and the creation of regions of disorder and order defined by the number of nearest-neighbour matches. A liquid crystalline globular phase provides a processable intermediate between water-soluble polymer and insoluble fibre. The reinforcement and matrix are both elements in a complex hierarchical microstructure that extends over length scales ranging from molecular to macroscopic. Collectively, this is responsible for the unique combination of mechanical properties exhibited by spider silk fibres.

The above discussion of silk fibres produced by spiders due to Viney,¹⁵ indicates how liquid crystalline order can be a precursor to the formation of the more ordered crystalline structures that become load bearing. We can see in nature combinations of the processes that are sometimes seen to occur individually in synthetic polymer systems.

A general discussion of the influence of chain conformation in copolymers on their ability to create specific structures has been presented elsewhere^{16,17} and indicates how local interactions lead to the creation of rod-like, helical and folded structures which are of crucial importance in nature achieving the structural feature that it requires for particular applications.

In summary, nature manages to combine the use of chemical complexity with kinetics and thermodynamics to produce materials that are fit for specific

purposes. Many of the principles that control the formation of structure and morphology in synthetic materials are demonstrated in a more diverse sense in naturally occurring materials. However, the same physical principles operate and are controlling the creation of these various structures. It is impossible in this short monograph to do justice to the wide variety of structures found in nature but hopefully the reader will recognize behind this plethora of morphologies some of the principal building blocks discussed in this book. Good hunting.

References

1. M. Er Rafik, F. Briki, M. Burghammer and J. Doucet, *J. Struct. Biol.*, 2006, **154**, 79.
2. S.-Y. Ding and M.E. Himmel, *J. Agric. Food Chem.*, 2006, **54**, 597.
3. C. Ververis, K. Georghiou, N. Christodoulakis, P. Santas and R. Santas, *Ind. Crops Products*, 2004, **19**, 245.
4. A.K. Bledzki and J. Gassan, *Prog. Polym. Sci.*, 1999, **24**, 221.
5. J. Einfeldt, D. Meissner and A. Kwasniewski, *Prog. Polym. Sci.*, 2001, **26**, 1419.
6. P. Zugenmeir, *Prog. Polym. Sci.*, 2001, **26**, 1341.
7. G.M. Brown and H.A. Ley, *Science*, 1965, **147**, 1038.
8. S.E. Doyle, A.M. Gibbons and R.A. Pethrick, in *Wood and Cellulose*, ed. J.F. Kennedy, G.O. Phillips, D.J. Wedlock and P.A. Williams, Ellis Harwood, Colchester, UK, 1987, ch. 7, p. 71.
9. C. Viney and A.H. Windle, in *Wood and Cellulose*, ed. J.F. Kennedy, G.O. Phillips, D.J. Wedlock and P.A. Williams, Ellis Harwood, Colchester, UK, 1987, ch. 8, p. 77.
10. K.C. Ellis and J.O. Warwicker, *J. Polym. Sci.*, 1962, **56**, 339.
11. J. Blackwell and R.H. Marchessault, in *Cellulose and Cellulose Derivatives*, ed. N.M. Bikales and L. Segal, Wiley Interscience, New York, 1971, part IV, p. 151.
12. R.A. Pethrick, S. Doyle, R.K. Harris, K.J. Packer and F. Heatley, *Polymer*, 1986, **27**, 19.
13. D.J. Crofton, S. Doyle and R.A. Pethrick, in *Wood and Cellulose*, ed. J.F. Kennedy, G.O. Phillips, D.J. Wedlock and P.A. Williams, Ellis Harwood, Colchester, UK, 1987, p. 237.
14. A.M. Emons and B.M. Mulder, *Trends Polym. Sci.*, 2000, **5**, 35.
15. C. Viney, *Supermolec. Sci.*, 1997, **4**, 75.
16. A. Tonelli and M. Srinivasarao, *Polymers from the Inside Out*, Wiley Interscience, Chichester, UK, 2001.
17. H. Zhu, J. Ji and J. Shen, *Biomacromolecules*, 2004, **5**, 1933.